

Resolved-Sideband Raman Cooling of a Bound Atom to the 3D Zero-Point Energy

C. Monroe, D. M. Meekhof, B. E. King, S. R. Jefferts, W. M. Itano, and D. J. Wineland

Time and Frequency Division, National Institute of Standards and Technology, Boulder, Colorado 80303

P. Gould

Department of Physics, University of Connecticut, Storrs, Connecticut 06269

(Received 19 December 1994)

We report laser cooling of a single ${}^9\text{Be}^+$ ion held in a rf (Paul) ion trap to where it occupies the quantum-mechanical ground state of motion. With the use of resolved-sideband stimulated Raman cooling, the zero point of motion is achieved 98% of the time in 1D and 92% of the time in 3D. Cooling to the zero-point energy appears to be a crucial prerequisite for future experiments such as the realization of simple quantum logic gates applicable to quantum computation.

PACS numbers: 32.80.Pj, 42.50.Vk, 42.65.Dr

Dramatic progress in the field of atomic laser cooling has provided cooling of free or weakly bound atoms to temperatures near the Doppler cooling limit [1], near the photon recoil limit [2], and, more recently, below the photon recoil limit [3,4]. For a tightly bound atom, a more natural energy scale is given by the quantized vibrational level n , where the energy is $E = \hbar\omega_v(n + \frac{1}{2})$ for an atom confined in a harmonic potential of frequency ω_v . In this case, the fundamental cooling limit is the $n = 0$ zero-point energy of the binding potential. In this Letter, we demonstrate a new technique for laser cooling a trapped atom to the 3D zero-point energy.

Attainment of the 3D ground state is significant for two primary reasons: (i) it appears to be a goal of intrinsic interest as it is the fundamental limit of cooling for a bound atom and approaches the ideal of an isolated particle at rest and (ii) it will be important in future planned experiments. For example, once the ion is cooled to the $n = 0$ state, it should be possible to realize the Jaynes-Cummings interaction [5] in the regime of strong coupling and generate other nonclassical states of motion such as squeezed states [6–8]. If the collective motion of two or more trapped ions can be cooled to the zero point, it may be possible to transfer correlation from the external motional state to the internal spin state of the ions. Generating “EPR”-like atomic spin states would not only be interesting from the point of view of quantum measurements [9], but may also allow a reduction of quantum noise in spectroscopy [6,7]. Zero-point cooling combined with long coherence times may make it possible to construct a quantum computer [10]. Cirac and Zoller have proposed a quantum computer based on a system of trapped ions, in which information is stored in the spin and motional states of the ions [11]. The fundamental switching action in this implementation of a quantum computer is a coherent exchange between the spin state of an individual ion and a collective vibrational state of all the ions. Cooling to the zero-point energy and realizing the Jaynes-Cummings coupling is critical to this scheme.

We cool a single beryllium ion bound in a rf (Paul) ion trap to near the zero-point energy using resolved-sideband laser cooling with stimulated Raman transitions along the lines suggested in Ref. [6]. The idea of resolved-sideband laser cooling with a single-photon transition is as follows [12]. Consider a two-level atom characterized by resonant transition frequency ω_0 and radiative linewidth γ . We assume the atom is confined by a 1D harmonic well of vibration frequency $\omega_v \gg \gamma$. If a laser beam (frequency ω_L) is incident along the direction of the atomic motion, the absorption spectrum is composed of a “carrier” at frequency ω_0 and resolved frequency-modulation sidebands spaced by ω_v , which are generated from the Doppler effect. Cooling occurs if the laser is tuned to a lower sideband, for example, at $\omega_L = \omega_0 - \omega_v$. In this case, photons of energy $\hbar(\omega_0 - \omega_v)$ are absorbed and spontaneously emitted photons of average energy $\hbar\omega_0$ return the atom to its initial internal state thereby reducing the atom’s kinetic energy by $\hbar\omega_v$ per scattering even (assuming $\hbar\omega_v$ is much greater than the photon recoil energy). Cooling proceeds until the atom’s mean vibrational quantum number in the harmonic well is given by $\langle n \rangle_{\min} \simeq (\gamma/2\omega_v)^2 \ll 1$ [1,13]. The interaction with the laser is significantly reduced once in the $n = 0$ state; thus the zero-point state satisfies the *operational definition* of a dark state [14] for γ/ω_v sufficiently small. Resolved-sideband cooling in 2D was previously achieved on a ${}^{198}\text{Hg}^+$ ion using a narrow single-photon optical quadrupole transition [15].

For laser cooling with stimulated Raman transitions [4,6,16,17], the single-photon transition is replaced by a stimulated Raman transition between metastable levels (e.g., hyperfine or Zeeman electronic ground state), and spontaneous Raman transitions irreversibly recycle the internal state of the atom. Stimulated Raman cooling offers the important practical advantages that the cooling linewidth can be varied experimentally, and the effective laser linewidth can be made very narrow by the use of optical frequency modulators. These features of stimu-

lated Raman cooling have already been used to achieve very low temperatures for free or weakly bound neutral atoms in the unresolved-sideband limit [4]. Since narrow single-photon transitions are not required, the resolved-sideband Raman cooling technique described here can be generalized to many ion species and may also be applied to strongly bound neutral atoms held in dipole traps [18] and optical lattices [19].

The experiment is conducted as follows. We first achieve $\langle n_v \rangle \approx 1$ in 3D ($v = x, y, z$) by performing Doppler cooling on an allowed electric dipole transition (γ large) and making the trap strong enough that $\omega_v \approx \gamma$. This Doppler “precooling” places the ion into the Lamb-Dicke regime ($\Delta x \ll \lambda/2\pi$, where Δx is the rms spread of the ion position and λ is the wavelength of the dipole transition). We reduce $\langle n_v \rangle$ further in 3D by employing a second stage of cooling on narrower Raman transitions between hyperfine ground states ($\gamma_{\text{Ram}} \ll \omega_v$). Finally we extract $\langle n_v \rangle$ by measuring the asymmetry of the resolved motional sidebands in the Raman absorption spectrum [15].

A single ${}^9\text{Be}^+$ ion is stored in a coaxial-resonator-based rf (Paul) ion trap ($r_0 \approx 170 \mu\text{m}$, $z_0 \approx 130 \mu\text{m}$) described in Ref. [20]. A potential $V_0 \cos(\Omega_0 t)$ is applied to the ring ($V_0 \approx 600 \text{ V}$, $\Omega_0/2\pi \approx 231 \text{ MHz}$), yielding ${}^9\text{Be}^+$ pseudopotential oscillation frequencies of $(\omega_x, \omega_y, \omega_z)/2\pi \approx (11.2, 18.2, 29.8) \text{ MHz}$ along the principal axes of the trap [21]. Once a ${}^9\text{Be}^+$ ion is loaded in the trap, its lifetime is about 6 h (background pressure $< 10^{-8} \text{ Pa}$).

The geometry and polarizations of the various laser beams as well as the relevant energy levels in ${}^9\text{Be}^+$ are summarized in Fig. 1. The quantization axis is defined by an applied magnetic field $|\mathbf{B}| \approx 0.18 \text{ mT}$. Laser radiation (beam $D2$, σ^+ polarized) detuned slightly to the red of the ${}^2S_{1/2}(F=2) \rightarrow {}^2P_{3/2}$ transitions ($\lambda \approx 313 \text{ nm}$, $\gamma/2\pi \approx 19.4 \text{ MHz}$, ${}^2P_{3/2}$ hyperfine structure $\approx 1 \text{ MHz}$) is directed at oblique angles to all the principal axes of the trap, providing Doppler precooling in all trap dimensions. A second 313 nm source (beam $D1$, σ^+ polarized) tuned to the ${}^2S_{1/2}(F=1) \rightarrow {}^2P_{3/2}$ transition prevents optical pumping to the $F=1$ ground state. A pair of Raman beams is also directed into the trap (beams $R1$ and $R2$) to drive a much narrower transition between the ${}^2S_{1/2} |F=2\rangle$ and $|F=1\rangle$ hyperfine ground states of ${}^9\text{Be}^+$ through the virtual ${}^2P_{1/2}$ state. The Raman beams are detuned $\approx 12 \text{ GHz}$ to the red of the ${}^2S_{1/2} \rightarrow {}^2P_{1/2}$ transition with a difference frequency very near the ${}^2S_{1/2}$ hyperfine splitting of $\omega_0/2\pi \approx 1.250 \text{ GHz}$. A third 313 nm source (beam $D3$, σ^+ polarized) is tuned to the ${}^2S_{1/2}(F=2) \rightarrow {}^2P_{1/2}(F=2)$ transition and depletes the $|F, m_F\rangle = |2, 1\rangle$ ground state. Beams $D1$, $D2$, and $D3$ are derived from two frequency-doubled dye lasers, producing 5–10 μW of power in each beam, enough to saturate the ion near resonance. Beams $R1$ and $R2$ are derived from a third frequency-doubled dye laser, providing a few mW of power in each

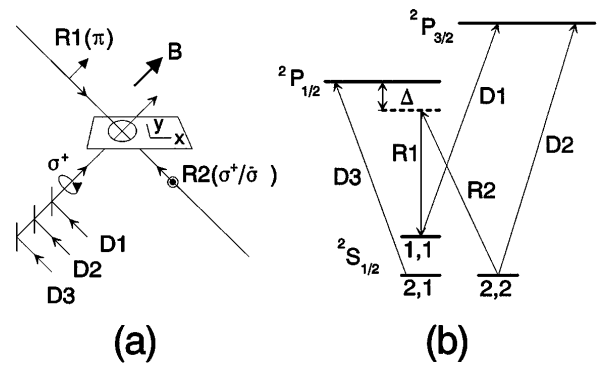


FIG. 1. (a) Laser beam geometry. The trap ring electrode (in the x - y plane) is shown rotated 45° into the page (the endcap electrodes along the z axis are not shown; see Ref. [20]). A magnetic field \mathbf{B} defines a quantization axis along $\hat{x}/\sqrt{2} + \hat{y}/2 + \hat{z}/2$, and laser beam polarizations are indicated. Fluorescence light is collected along the direction perpendicular to the page. (b) Relevant ${}^9\text{Be}^+$ energy levels (not to scale), indicated by F, m_F , quantum numbers in the ${}^2S_{1/2}$ ground state (2P fine-structure splitting is $\approx 197 \text{ GHz}$, ${}^2S_{1/2}$ hyperfine splitting is $\omega_0/2\pi \approx 1.250 \text{ GHz}$, and the ${}^2P_{3/2}$ hyperfine and Zeeman structure is not resolved). All optical transitions are near $\lambda \approx 313 \text{ nm}$. $D1$ and $D2$: Doppler precooling and detection beams; $D3$: $|2, 1\rangle$ depletion beam; $R1$ and $R2$: Raman beams. The detuning of $R1$ and $R2$ from the ${}^2S_{1/2} \rightarrow {}^2P_{1/2}$ transition is $\Delta/2\pi \approx 12 \text{ GHz}$.

beam. The difference frequency of the Raman beams is tunable over the range 1200–1300 MHz with the use of a double-pass acousto-optic modulator (AOM). The counterpropagating Raman beams are also at oblique angles to the trap’s principal axes and are therefore sensitive to motion in all dimensions. All beams are shuttered with AOMs. The 313 nm fluorescence from the trapped ion is imaged through $f/2$ optics onto a position-sensitive photomultiplier tube, resulting in a photon count rate as high as $\approx 10 \text{ kHz}$ (quantum efficiency $\approx 2 \times 10^{-4}$). The background count rate is $\approx 100 \text{ Hz}$.

Doppler precooling, Raman cooling, and measurement of the Raman absorption spectrum are accomplished by following the sequence outlined in Table I. After precooling (beams $D1$, $D2$, and $D3$), the ion is prepared in the ${}^2S_{1/2}|2, 2\rangle$ electronic ground state by turning off beam $D2$. The relative tuning of the Raman beams is set to a first lower (red) sideband near $\omega_0 - \omega_v$, driving a stimulated Raman transition from the $|2, 2\rangle |n_v\rangle$ state to the $|1, 1\rangle |n_v - 1\rangle$ state. The ion is then recycled with nearly resonant beams $D1$ and $D3$, inducing spontaneous Raman transitions predominantly to the $|2, 2\rangle |n_v - 1\rangle$ state. This cycling of stimulated and spontaneous Raman transitions (steps 3 and 4 of Table I) is repeated as desired on any or all of the three dimensions. The relative tuning of the Raman beams is then set near $\omega_0 + \delta_{\text{pr}}$, and a stimulated Raman “probe” transition is driven between the states, where $\Delta n_v = 0, \pm 1$. The probability of driving the probe transition is then measured by

driving a stimulated Raman “exchange π pulse” from $|2, 2\rangle |n_v\rangle \leftrightarrow |1, 1\rangle |n_v\rangle$, followed by driving the cycling $^2S_{1/2}|2, 2\rangle \rightarrow ^2P_{3/2}|3, 3\rangle$ transition with beam $D2$ and gating and collecting the fluorescence. (The exchange π pulse in step 6 of the table reduces the fluorescence noise when $\langle n_v \rangle \approx 0$.) The ion scatters thousands of photons on the cycling transition before decaying into the $|1, 1\rangle$ electronic state due to imperfect circular polarization of beam $D2$, resulting in a net quantum efficiency near 1. As this sequence is repeated at ≈ 4 kHz, δ_{pr} is slowly swept, yielding the Raman absorption spectrum.

The Raman carrier represents the transition $|2, 2\rangle |n_v\rangle \leftrightarrow |1, 1\rangle |n_v\rangle$ and occurs at $\delta_{pr} \equiv 0$ (compensating for stable Zeeman and ac Stark shifts of ≈ 2 MHz). In the Lamb-Dicke regime, the carrier feature has strength $I_c = \sin^2(\Omega \tau_{pr})$, where $\Omega = g_1 g_2 / \Delta$ is the carrier Rabi flopping frequency, τ_{pr} is the exposure time of the atom to the probe Raman beams, g_1 and g_2 are the resonant Rabi frequencies of Raman beams $R1$ and $R2$, and Δ is the detuning of the Raman beams from the excited state (we assume $\Delta \gg \gamma, g_1, g_2$) [6]. In each dimension, blue and red sidebands occurring at $\delta_{pr} = \pm \omega_v$ represent the transitions $|2, 2\rangle |n_v\rangle \leftrightarrow |1, 1\rangle |n_v \pm 1\rangle$. The strengths of the blue and red sidebands in the Lamb-Dicke regime are given by $I_v^{\text{blue}} = \langle \sin^2[\Omega \tau_{pr} \eta_v (n_v + 1)^{1/2}] \rangle$ and $I_v^{\text{red}} = \langle \sin^2[\Omega \tau_{pr} \eta_v n_v^{1/2}] \rangle$, where the average is performed over the distribution of n_v . The Lamb-Dicke parameters are given by $\eta_v = \delta k_v r_v = (0.21, 0.12, 0.09)$, where $\delta k_v = 2k_v$ is the component of the difference in the counterpropagating Raman beam wave vectors in the v th dimension, and $r_v = (\hbar/2m\omega_v)^{1/2}$ is the spread of the $n_v = 0$ wave function. The sideband Rabi flopping frequencies $\Omega \eta_v$ are typically a few hundred kilohertz, thus the absorption features are well resolved and spontaneous emission during all stimulated Raman processes is negligible.

A Raman absorption spectrum of the first blue and red sidebands of the x direction ($\delta_{pr} = \pm \omega$) is shown in Fig. 2 (solid points) for Doppler precooling only (omitting steps 3 and 4 in Table I). Similar features appear at $\delta_{pr} = \pm \omega_y$ and $\pm \omega_z$. If n_v is thermally distributed, then it is straightforward to show that $I_v^{\text{red}}/I_v^{\text{blue}} = \langle n_v \rangle / (1 + \langle n_v \rangle)$, independent of $\Omega \tau_{pr} \eta_v$. By recording several spectra varying τ_{pr} , we find the ratio of red to blue sideband strength remains approximately constant, indicating a nearly thermal distribution of n_v . (We ensure that Ω is the same on the blue and red sidebands.) We measure $\langle n_v \rangle$ for a variety of red detunings of Doppler precooling beams $D1$ and $D2$ and obtain values as low as $\langle n_v \rangle \approx (0.47, 0.30, 0.18)$ in the three dimensions at a detuning of about -30 MHz (we estimate $\approx 10\%$ uncertainties in the measurements). At other detunings, we measure values as high as $\langle n_v \rangle \approx 7$. These values and their behavior with detuning are consistent with the theoretical limit of Doppler cooling [17].

Figure 2 includes a Raman absorption spectrum following additional sideband Raman cooling (hollow points). Five Raman cooling cycles in the x dimensions are em-

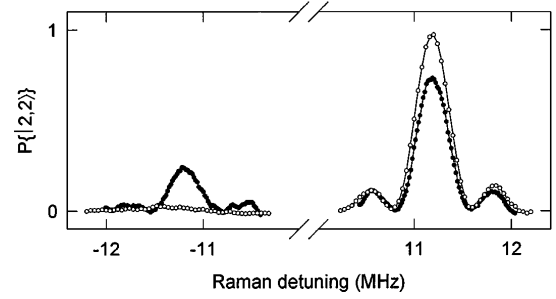


FIG. 2. Raman absorption spectrum of a single $^9\text{Be}^+$ ion after Doppler precooling (solid points) and after five cycles of additional resolved sideband stimulated Raman cooling on the x dimension (hollow points). The observed count rate is normalized to the probability $P\{|2, 2\rangle\}$ of the ion being in the $|2, 2\rangle$ state. The first blue and red sidebands of the x dimension are shown at $\delta_{pr}/2\pi \approx \pm 11.2$ MHz. Similar sidebands are found near ± 18.2 MHz (y dimension) and at ± 29.8 MHz (z dimension). For precooling, the asymmetry in the sidebands indicates a thermal average vibrational occupation number of $\langle n_x \rangle \approx 0.47(5)$. For Raman cooling, the reduction of the red sideband and growth of the blue sideband implies further Raman cooling in the x dimension to $\langle n_x \rangle \approx 0.014(10)$. The widths of the features are consistent with the $2.5 \mu\text{s}$ Raman probe time. Each point represents an average of 400 measurements, corresponding to ≈ 5 min of integration time for the entire data set. The lines connect the data points.

ployed (steps 3 and 4 of Table I with $\omega_v = \omega_x$). The exposure time τ_{Ram} of the last Raman pulse is set so that $\Omega \tau_{\text{Ram}} \eta_x \approx \pi/2$ or $\tau_{\text{Ram}} \approx 2.5 \mu\text{s}$, corresponding to nearly a π pulse from the $n_x = 1$ state to the $n_x = 0$ state. The durations of the earlier pulses are set shorter to optimize the cooling. The recycle time between each stimulated Raman transition is about $7 \mu\text{s}$, ample time for the ion to scatter the expected average of ≈ 3 photons from beams $D1$ and $D3$ and ultimately get recycled to the $|2, 2\rangle$ state. The suppression of the red sideband (and growth of the blue sideband) indicates the extent of the additional cooling, from $\langle n_x \rangle \approx 0.47$ to $\langle n_x \rangle \approx 0.014(10)$ (the $n_x = 0$ state is occupied $\approx 98\%$ of the time). We observe no further cooling by increasing the number of Raman cooling cycles beyond about five and see little sensitivity to the details of the Raman cooling pulse durations. As discussed above, we verify that the distribution of n_v is nearly thermal after Raman cooling. We achieve resolved-sideband Raman cooling in 3D by sequentially driving on all three red sidebands. Five cycles of cooling are applied to each dimension (order $xyzxyz \dots$) by alternating the tuning of the Raman cooling beams between the three red sidebands. From the measured asymmetry of each pair of sidebands, we infer 3D Raman cooling to $\langle n_v \rangle \approx (0.033, 0.022, 0.029)$, or the $n_x = n_y = n_z = 0$ 3D ground state being occupied $\approx 92\%$ of the time.

The limit of Raman cooling is determined by heating from off-resonant stimulated-Raman transitions [expected to result in a limit of $\langle n_x \rangle_{\text{St Ram}} \approx (g_1 g_2)^2 / (\omega_v \Delta)^2 \approx$

TABLE I. Timing sequence for Doppler precooling, resolved-sideband stimulated Raman cooling and Raman detection of $\langle n_v \rangle$. As the sequence is repeated through steps 1–7, δ_{pr} is slowly swept across absorption features. Raman cooling steps (3 and 4) are repeated as desired within the sequence.

Step	Duration (μ s)	Beams $D1, D3$	$D2$	$R1, R2$	Raman tunning	Function
1	≈ 50	On	On	Off	...	Doppler precool
2	≈ 7	On	Off	Off	...	Prepare in $ 2, 2\rangle$ state
3	1–3	Off	Off	On	$\omega_0 - \omega_v$	Stimulated Raman transition $ 2, 2\rangle n_v\rangle \rightarrow 1, 1\rangle n_v - 1\rangle$
4	≈ 7	On	Off	Off	...	Spontaneous Raman recycle $ 1, 1\rangle n_v - 1\rangle \rightarrow 2, 2\rangle n_v - 1\rangle$
5	1–3	Off	Off	On	$\omega_0 + \delta_{pr}$	Probe $\langle n_v \rangle$ with stimulated Raman transitions $ 2, 2\rangle n_v\rangle \rightarrow 1, 1\rangle n'_v\rangle$
6	≈ 1	Off	Off	On	ω_0	Exchange π pulse: $ 2, 2\rangle n_v\rangle \leftrightarrow 1, 1\rangle n_v\rangle$
7	≈ 200	Off	On	Off	...	Detect transition in step 5: cycle on $ 2, 2\rangle \rightarrow 3, 3\rangle$; collect fluorescence

10^{-3}] and heating from off-resonant spontaneous emission from the Raman beams [a limit of $\langle n_x \rangle_{\text{Sp Ram}} \approx (g_1 g_2 / \Delta^2) \eta_x \gamma \tau_{\text{Ram}} \approx 10^{-3}$]. We believe the minimum measured value of $\langle n_x \rangle \approx 0.02$ may be due to anomalous heating of the ion, which we measure to be $\partial \langle n \rangle / \partial t \approx +1/\text{msec}$ by inserting various amounts of time between cooling probing. We are currently investigating the source of this heating.

This work is supported by the Office of Naval Research and the Army Research Office. We acknowledge considerable contributions from J. C. Bergquist. We thank N. R. Newbury, J. D. Miller, and M. Young for comments on the manuscript.

- [1] D. J. Wineland and W. M. Itano, *Phys. Today* **40**, No. 6, 34 (1987).
- [2] C. Cohen-Tannoudji and W. D. Phillips, *Phys. Today* **43**, No. 10, 33 (1990).
- [3] A. Aspect, E. Arimondo, R. Kaiser, N. Vansteenkiste, and C. Cohen-Tannoudji, *Phys. Rev. Lett.* **61**, 826 (1988); J. Lawall, F. Bardou, B. Saubamea, M. Leduc, A. Aspect, and C. Cohen-Tannoudji, *Phys. Rev. Lett.* **73**, 1915 (1994).
- [4] M. Kasevich and S. Chu, *Phys. Rev. Lett.* **69**, 1741 (1992); H. Lee, C. Adams, N. Davidson, B. Young, M. Weitz, M. Kasevich, and S. Chu, in *Atomic Physics XIV*, edited by D. J. Wineland, C. E. Wieman, and S. J. Smith (AIP Press, New York, 1995), p. 258.
- [5] E. T. Jaynes and C. W. Cummings, *Proc. IEEE* **51**, 89 (1963).
- [6] D. J. Heinzen and D. J. Wineland, *Phys. Rev. A* **42**, 2977 (1990).
- [7] D. J. Wineland, J. J. Bollinger, W. M. Itano, and D. J. Heinzen, *Phys. Rev. A* **50**, 67 (1994).
- [8] J. I. Cirac, A. S. Parkins, R. Blatt, and P. Zoller, *Phys. Rev. Lett.* **70**, 556 (1993); J. I. Cirac, R. Blatt, A. S. Parkins, and P. Zoller, *Phys. Rev. Lett.* **70**, 762 (1993).
- [9] D. M. Greenberger, M. A. Horne, and A. Zeilinger, *Phys. Today* **46**, No. 8, 22 (1993).
- [10] A. Ekert, in *Atomic Physics XIV*, edited by D. J. Wineland, C. E. Wieman, and S. J. Smith (AIP Press, New York,

- 1995), p. 450, and references therein.
- [11] J. I. Cirac and P. Zoller, *Phys. Rev. Lett.* **74**, 4091 (1995).
- [12] D. J. Wineland and H. Dehmelt, *Bull. Am. Phys. Soc.* **20**, 637 (1975).
- [13] W. Neuhauser, M. Hohenstatt, P. Toschek, and H. Dehmelt, *Phys. Rev. Lett.* **41**, 233 (1978).
- [14] R. Dum, P. Marte, T. Pellizari, and P. Zoller, *Phys. Rev. Lett.* **73**, 2829 (1994).
- [15] F. Diedrich, J. C. Bergquist, W. M. Itano, and D. J. Wineland, *Phys. Rev. Lett.* **62**, 403 (1989).
- [16] P. E. Toschek, *Phys. (Paris)* **10**, 761 (1985); H. Dehmelt, G. Janik, and W. Nagourney, *Bull. Am. Phys. Soc.* **30**, 111 (1985); B. Appasamy, I. Siemers, Y. Stalgies, J. Eschner, R. Blatt, W. Neuhauser, and P. E. Toschek, *Appl. Phys. B* **60**, 473 (1995).
- [17] M. Lindberg and J. Javanainen, *J. Opt. Soc. Am. B* **3**, 1008 (1986).
- [18] S. Chu, J. E. Bjorkholm, A. Ashkin, and A. Cable, *Phys. Rev. Lett.* **57**, 314 (1986); W. D. Phillips, in *Laser Manipulation of Atoms and Ions*, Proceedings of the International School of Physics “Enrico Fermi,” Varenna, 1991, edited by E. Arimondo and W. D. Phillips (North-Holland, Amsterdam, 1992), p. 325; J. D. Miller, R. A. Cline, and D. J. Heinzen, *Phys. Rev. A* **47**, R4567 (1993).
- [19] P. Verkerk, B. Lounis, C. Salomon, and C. Cohen-Tannoudji, *Phys. Rev. Lett.* **68**, 3861 (1992); P. Jessen, C. Gerz, P. Lett, W. Phillips, S. Rolston, R. Spreuw, and C. Westbrook, *Phys. Rev. Lett.* **69**, 49 (1992); A. Hemmerich and T. Hänsch, *Phys. Rev. Lett.* **70**, 410 (1993).
- [20] S. R. Jefferts, C. Monroe, E. Bell, and D. J. Wineland, *Phys. Rev. A* **51**, 3112 (1995).
- [21] The drive frequency $\Omega_0 \approx 231$ MHz is much larger than the pseudopotential vibration frequencies ω_v , so the contribution of the driven “micromotion” at Ω_0 to the overall amplitude of the ion motion is very small. This includes the micromotion induced from static background fields, which are minimized with compensation electrodes (see Ref. [20]). Moreover the small FM micromotion sidebands at $\pm\Omega_0$ are well resolved ($\Omega_0 \gg \gamma$) and far from the region of interest in the absorption spectrum. Thus the trap can be accurately approximated as a simple harmonic oscillator with frequencies ω_v .